J. Fluid Mech. (1992), *vol.* 234, *pp.* 651–667
Printed in Great Britain

Higher harmonic resonance of two-dimensional disturbances in Rayleigh–Bénard convection

By JIRO MIZUSHIMA[1] AND KAORU FUJIMURA[2]

[1]Faculty of Education, Wakayama University, Wakayama 640, Japan
[2]Japan Atomic Energy Research Institute, Tokai-mura, Ibaraki 319-11, Japan

(Received 5 November 1990 and in revised form 30 July 1991)

A higher harmonic resonance with wavenumber ratio of 1 : 3 is found to take place in Rayleigh–Bénard convection under rigid–rigid boundary conditions. Bifurcation diagrams for two-dimensional motion are obtained for various values of the Prandtl number P. It is found that a pure mode and mixed mode solutions exist as nonlinear equilibrium states of primary roll solutions for relatively high-Prandtl-number fluids ($P \geqslant 0.13$) while the pure mode, mixed modes, travelling wave and modulated wave solutions exist for relatively low-Prandtl-number fluids ($P \leqslant 0.12$).

1. Introduction

Pattern selection in the convection in a fluid layer heated from below has been investigated extensively by Schlüter, Lortz & Busse (1965), Busse (1967), Clever & Busse (1974), and Busse & Clever (1979). They calculated the steady primary roll solutions and examined in detail their linear stability to additional two-dimensional or three-dimensional disturbances. Their results show that the primary rolls are unstable to many types of secondary instabilities such as zigzag, cross-roll, Eckhaus, oscillatory, knot, and skewed varicose, which occur depending on the values of the parameters. The stability boundaries to these instability modes are collected in one diagram called Busse's balloon. All the instabilities predicted were experimentally confirmed to occur by Busse & Whitehead (1971).

For the monochromatic and steady primary roll, the stability boundaries for the secondary instabilities are thus well understood now. This is not however the case if the primary solutions are neither monochromatic nor steady as we will discuss in a later section. The latter situation occurs at high Rayleigh number where multiple mode interactions take place.

The multiple mode interaction in Rayleigh–Bénard convection was investigated by Kidachi (1982) and Knobloch & Guckenheimer (1983) where two modes bifurcate from the conduction state simultaneously or successively. They analysed the nonlinear interaction between two modes of k-rolls and $(k+1)$-rolls in a finite rectangular domain with stress-free boundaries and derived a set of amplitude equations, i.e. coupled Landau equations, for the two modes. They found that the transition between two sets of rolls occurs through the generation of a mixed mode for low Prandtl numbers while it occurs through rather abrupt transition involving hysteresis for high Prandtl numbers. It is noted here that the nonlinear interaction between the two modes is not a resonant interaction, but an interaction mainly through mean field deformation and that the effect of the phase difference does not enter there because the derivation of the equations was truncated at the cubic order.

Busse & Or (1986) obtained a new class of solutions which do not reflect the symmetry of the physical conditions. They extended the analysis to a higher-order solution, including the effect of the phase difference between the two modes, and obtained a new type of mixed mode solution which is distinguished from the one obtained by Knobloch & Guckenheimer by a tilt of the convection rolls. The new type of mixed mode solution shares with Knobloch & Guckenheimer's one the property that it is unstable for large Prandtl numbers and becomes stable for Prandtl numbers $P \leqslant 0.296$.

Armbruster (1987) derived fifth-order bifurcation equations as the normal form which is equivariant under an action of $O(2) \times Z(2)$-symmetry groups. He then showed how the different types of solutions of Knobloch & Guckenheimer and of Busse & Or arise. He introduced free phases in the interacting modes. He found two types of mixed mode solutions and a travelling wave solution as well as the pure mode ones. All the interesting new solutions are unfortunately unstable.

Busse (1987) further extended the work of Busse & Or by focusing attention on the effect of a small quadratic dependence of the density on the temperature. This situation breaks the spatial symmetry which would be present in the conventional treatment of Rayleigh–Bénard convection with density having linear dependence on temperature, so that 1:2 resonance can take place at the quadratic order. He obtained coupled amplitude equations and demonstrated how drastically the bifurcation characteristics are changed by the resonance mechanism.

Similar nonlinear interactions between stationary modes have been investigated for other fluid flows. Nagata & Busse (1983) and Mizushima & Saito (1988) examined the nonlinear stability of free convection in a vertical slot with sidewall heating. They showed that the parameter range in which a two-dimensional nonlinear equilibrium solution exists differs from a linearly unstable domain. Fujimura & Mizushima (1987) derived the coupled amplitude equations and clarified that this rather contradictory phenomenon is due to nonlinear 1:2 resonance. Meyer-Spasche & Keller (1985), Li (1986), Specht, Wagner & Meyer-Spasche (1989) also reported the 1:2 resonance for Couette flow between rotating concentric cylinders with different speeds.

Many complicated and interesting nonlinear interactions appeared as the multiple bifurcations were analysed in a unified manner by Dangelmayr (1986) and Dangelmayr & Armbruster (1986). Under the presence of $O(2)$-symmetry, they derived the normal forms for two interacting stationary modes with $m:n$ resonance and obtained bifurcation diagrams for various cases, especially for $m \geqslant 2$ and $(m:n) = (1:2)$. Their theory assumes only $O(2)$-symmetry and may be applicable to various fluid motions having periodic boundary conditions.

The objective of the present paper is to investigate the bifurcation of solutions with 1:3 resonance in Rayleigh–Bénard convection mainly for the parameter range in which Clever & Busse encountered the difficulty in their evaluation of the primary roll solutions (see Nagata & Busse for the difficulty). The resonance takes place in the Rayleigh–Bénard convection between rigid–rigid boundaries reflecting the symmetry of the physical conditions of the convection layer with periodic lateral boundary conditions. We will obtain global bifurcation diagrams for a relatively large Prandtl number. We will also derive coupled amplitude equations over a wide range of the Prandtl number. The equations, a subset of the general form obtained by Dangelmayr and Dangelmayr & Armbruster, possess pure mode, mixed mode, travelling wave, and modulated travelling wave solutions depending on the value of the Prandtl number. The local equations will be shown to well reproduce the global characteristics. We will further discuss the effect of the resonance on the bifurcation diagram expressed by Busse's balloon and on the interpretation of the balloon.

2. Nonlinear equilibrium solution for two-dimensional primary roll disturbances

Suppose that a gap between two horizontal parallel plates at different temperatures is filled with a fluid. We confine ourselves to two-dimensional flows and take a Cartesian system of coordinates with x and z as the horizontal and vertical directions opposite to the direction of gravity, respectively. Making use of the Boussinesq approximation and introducing the stream function ψ in the (x, z)-plane, the governing equations of the stream function ψ and deviation T of the temperature from heat conduction state are written in a standard non-dimensional form as

$$\frac{\partial \nabla^2 \psi}{\partial t} - P\nabla^4\psi + PR\frac{\partial T}{\partial x} = J(\psi, \nabla^2\psi), \tag{1}$$

$$\frac{\partial T}{\partial t} + \frac{\partial \psi}{\partial x} - \nabla^2 T = J(\psi, T), \tag{2}$$

where R is the Rayleigh number, P is the Prandtl number, $J(f, g)$ is the Jacobian defined by

$$J(f,g) \equiv \frac{\partial(f,g)}{\partial(x,z)},$$

and ∇^2 is the two-dimensional Laplacian in the (x, z)-plane defined by

$$\nabla^2 \equiv \frac{\partial^2}{\partial x^2} + \frac{\partial^2}{\partial z^2}.$$

The boundary conditions for ψ and T are written as

$$\frac{\partial \psi}{\partial x} = \frac{\partial \psi}{\partial z} = T = 0 \quad \text{at} \quad z = \pm\tfrac{1}{2}. \tag{3}$$

The linear stability of Rayleigh–Bénard convection has been investigated by Jeffreys (1928), Pellew & Southwell (1940), and Reid & Harris (1958). It is known that the principle of exchange of stability holds for this problem so that the phase velocity of a growing disturbance wave, if it exists, is zero. The most unstable disturbance has a spatial structure which is symmetric with respect to the midplane $z = 0$. We depict the neutral stability curve in figure 1 by a curve connecting the closed circles. The curve on the left-hand side is also the neutral curve but is depicted by scaling the wavenumber α by $\frac{1}{3}$ for later reference. Our careful numerical calculation reveals that the critical Rayleigh number R_c and the critical wavenumber α_c are given by $R_c = 1707.762$ and $\alpha_c = 3.1163236$.

To obtain the nonlinear equilibrium solutions of the two-dimensional primary roll, we expand ψ and T in Fourier series in the x-direction as

$$\psi = \sum_{n=-\infty}^{\infty} \phi_n \, \mathrm{e}^{\mathrm{i}n\alpha x}, \quad T = \sum_{n=-\infty}^{\infty} \theta_n \, \mathrm{e}^{\mathrm{i}n\alpha x}. \tag{4}$$

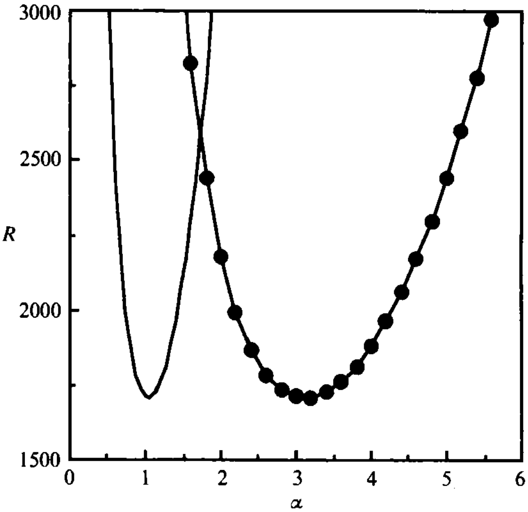

FIGURE 1. Neutral stability curve. It is independent of the Prandtl number. The curve on the left-hand side is also the neutral stability curve but is depicted by reducing the scale of α by $\frac{1}{3}$.

The ϕ_n are pure imaginary and $\phi_{-n} = -\phi_n$ holds, while the θ_n are pure real and $\theta_{-n} = \theta_n$ holds. Equations for the Fourier coefficients ϕ_n and θ_n are given by

$$\frac{\partial S_n \phi_n}{\partial t} - PS_n^2 \phi_n + \mathrm{i}n\alpha PR\theta_n = \sum_{p+q=n} \mathrm{i}\alpha[p\phi_p S_q \mathrm{D}\phi_q - q\mathrm{D}\phi_p S_q \phi_q], \tag{5}$$

$$\frac{\partial \theta_n}{\partial t} + \mathrm{i}n\alpha\phi_n - S_n \theta_n = \sum_{p+q=n} \mathrm{i}\alpha[p\phi_p \mathrm{D}\theta_q - q\mathrm{D}\phi_p \theta_q], \tag{6}$$

where $\mathrm{D} \equiv \mathrm{d}/\mathrm{d}z$ and $S_n \equiv \mathrm{D}^2 - n^2\alpha^2$. Here we truncated the Fourier expansions at $n = \pm N$. We further set $\partial/\partial t = 0$ in order to obtain the steady equilibrium solutions. As stated above, the most unstable disturbance on the linear basis has even symmetry in the z-direction. Symmetry consideration of the nonlinear terms in (5) and (6) indicates that two modes with the same symmetry induce an antisymmetric mode through the nonlinear interaction, whereas two modes with opposite symmetry induce a symmetric mode. Let us take an even symmetric disturbance as the fundamental mode ($n = 1$). The symmetric odd-order harmonic modes ($n = 3, 5, \ldots$) and the antisymmetric even-order harmonic modes ($n = 2, 4, \ldots$) can thus constitute a subset of the solutions. Although all the solutions which exist in the neighbourhood of the criticality are contained in this subset, more general solutions not contained in the subset might also be realized far from the criticality. We, however, restrict ourselves to the analysis of the subset and assume that the even-order harmonic has odd symmetry while the odd-order harmonic has even symmetry in order to compare the results shown below with the previous results like the ones by Busse and his coworkers. In the Appendix, we will violate this assumption by introducing an even symmetric second harmonic mode. Under this assumption, we expand ϕ_n and θ_n in Chebyshev polynomials as

$$\phi_n = \mathrm{i} \sum_{m=0}^{M+3} a_{nm}(1-(2z)^2)^2 T_m(2z), \quad \theta_n = \sum_{m=0}^{M+3} b_{nm}(1-(2z)^2) T_m(2z). \tag{7}$$

Here $T_n(2z)$ is the Chebyshev polynomial of the nth degree, and a_{nm} and b_{nm} vanish if

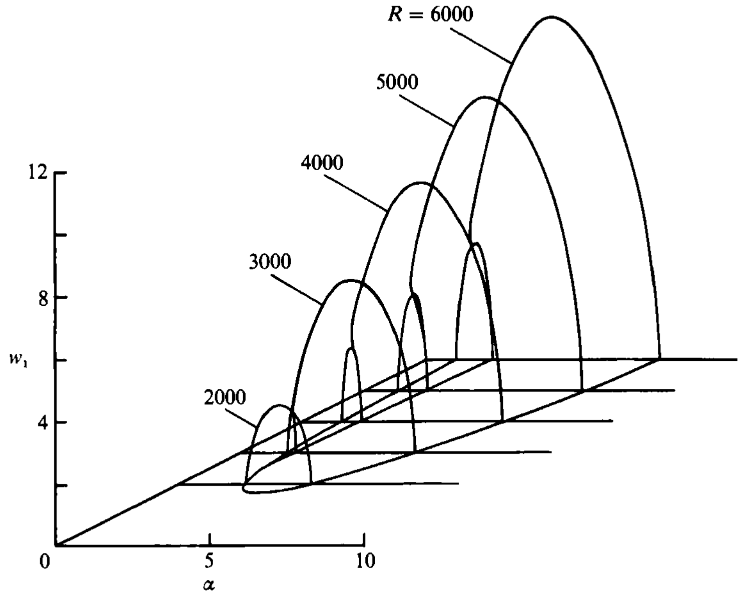

FIGURE 2. Distribution of the nonlinear equilibrium amplitude at $z = 0$, $w_1 \equiv \mathrm{i}\alpha\phi_1$. $P = 7.0$.

R	Nu (Clever & Busse)	Nu (Present result)
2000	1.214	1.21292
2500	1.478	1.47502
3000	1.667	1.66250
5000	2.112	2.10299
10000	2.618	2.60790
20000	3.119	3.10686
30000	3.440	3.42016
50000	3.894	3.85185

TABLE 1. Comparison of the present results with those of Clever & Busse (1974). $\alpha_c = 3.117$, $P = 7.0$

both of n and m are odd or even. Substitution of (7) into (5) and (6), assumption of $\partial/\partial t = 0$, and utilization of the collocation method yield algebraic equations for $2(N+1)(M+4)$ real coefficients a_{nm} and b_{nm}. The nonlinear equations were solved based on the Newton–Raphson method.

Prior to showing the results of nonlinear equilibrium solutions, let us compare the present numerical results with those of Clever & Busse (1974). In table 1, we tabulate the comparison of the values of the Nusselt number for $P = 7.0$ (water) at critical wavenumber $\alpha_c = 3.117$. (Precisely, the more accurate value of α_c is 3.1163236, but we utilized the former value for the comparison with Clever & Busse's results.) Expansions in Fourier series and Chebyshev polynomials are truncated at $N = 12$ and $M = 30$, respectively. Other than the fact that the present results are more accurate than Clever & Busse's, both are almost the same. Our claim that the present results are more accurate is because the truncation levels in the present paper, N and M, are larger than those taken in Clever & Busse's paper.

We show in figure 2 the equilibrium amplitude of the vertical velocity component $w_1 \equiv \mathrm{i}\alpha\phi_1$ at $z = 0$ for the primary roll with $P = 7.0$. The figure shows that the

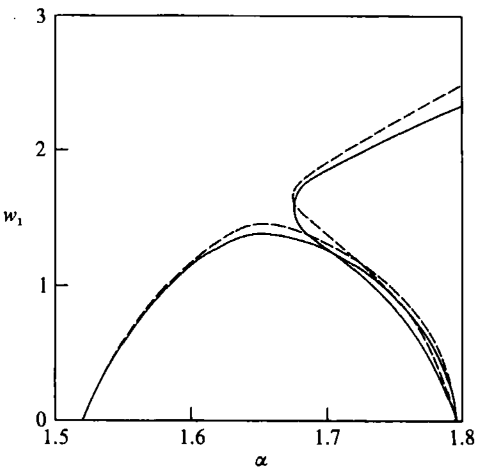

FIGURE 3. Comparison of equilibrium amplitudes obtained from two methods on an enlargement of figure 2 around $\alpha = 0.17$ for $R = 3000$. Solid line: Fourier truncation method, dashed line: weakly nonlinear theory.

equilibrium amplitude is given by a single curve for $R = 2000$ while the amplitude is given by two curves for $R \geqslant 3000$. Linear stability theory can only predict the situation where the equilibrium amplitude is given by a single curve like the one for $R = 2000$.

The curves for $1.5 \leqslant \alpha \leqslant 1.8$ in figure 2 are enlarged in figure 3 for $R = 3000$ in order to show the detail at the place where the two curves meet. It is found from the figure that three equilibrium solutions co-exist in the neighbourhood of $\alpha = 1.7$. This point has been overlooked in the many previous investigations of Rayleigh–Bénard convection; that is, secondary instability has been examined for primary roll solutions by assuming that the roll solutions uniquely exist in all the linear unstable domain.

3. Local bifurcation analysis

We obtained the global bifurcation diagrams for two-dimensional primary roll solutions in the previous section for relatively large Prandtl number fluids. Local bifurcation diagrams for various values of the Prandtl number, on the other hand, will be obtained in this section.

According to the ordinary weakly nonlinear stability theory for a monochromatic mode, the temporal evolution of the complex amplitude A_1 for the fundamental mode ($\alpha = \alpha_1$) is governed by a Landau equation of the form of

$$\frac{\mathrm{d}A_1}{\mathrm{d}t} = \lambda_1 A_1 + \lambda_{-111} |A_1|^2 A_1, \tag{8}$$

if the equation is truncated at the cubic order. Coefficients involved in (8) are pure real for the present problem. This equation guarantees that a growing disturbance with $\lambda_1 > 0$ approaches the equilibrium amplitude $|A_1|_{\mathrm{eq}} = (-\lambda_1/\lambda_{-111})^{\frac{1}{2}}$ if $\lambda_{-111} < 0$. Near the critical Rayleigh number, (8) holds for $\alpha_1 \approx \alpha_c$ without any influence of the higher harmonic resonance that is discussed below. The equilibrium amplitude of the vertical velocity component at $z = 0$, $w_1 \equiv \alpha_1 |A_1|_{\mathrm{eq}}$, is calculated for $P = 7.0$ based

R	w_1 (weakly nonlinear)	w_1 (Fourier truncation)
1710	0.214244	0.214122
1720	0.502383	0.500831
1750	0.941117	0.931211
1800	1.40973	1.37800
1900	2.08888	1.99476
2000	2.63995	2.46596
2200	3.58719	3.21677
2400	4.43589	3.83331
2600	5.23353	4.37230
2800	5.99985	4.85923
3000	6.74491	5.30812

TABLE 2. Comparison of the magnitude of w_1 obtained using weakly nonlinear theory and Fourier truncation method. $\alpha_c = 3.1163236$, $P = 7.0$

on the amplitude expansion method and is shown in table 2 with numerical results based on the Fourier truncation method described in the previous section. Numerical values calculated on the basis of (8) are found to be almost correct around the critical Rayleigh number, but deviate from the accurate value obtained from the Fourier truncation method as the Rayleigh number increases.

As we described in the previous sections, unstable disturbances in Bénard convection have spatial symmetry in the z-direction and two modes with the same symmetry induce an antisymmetric mode through the nonlinear interaction, whereas two modes with opposite symmetry induce a symmetric mode. So, it is expected that the symmetric fundamental mode ($\alpha = \alpha_1$) and the symmetric third harmonic mode ($\alpha = 3\alpha_1$) can resonate with each other for particular sets of parameters. Figure 1 guarantees that the exact resonance occurs between the neutral fundamental mode with $\alpha = 1.7232445$ and $R = 2573.739$ and its third harmonic. Taking account of the effect of this higher harmonic resonance, one can obtain a set of coupled amplitude equations using the weakly nonlinear stability theory based on the method of multiple scales:

$$\frac{\mathrm{d}A_1}{\mathrm{d}t} = \lambda_1 A_1 + \lambda_{-111}|A_1|^2 A_1 + \lambda_{-331}|A_3|^2 A_1 + \lambda_{-1-13} A_1^{*2} A_3, \tag{9}$$

$$\frac{\mathrm{d}A_3}{\mathrm{d}t} = \lambda_3 A_3 + \lambda_{-113}|A_1|^2 A_3 + \lambda_{-333}|A_3|^2 A_3 + \lambda_{111} A_1^3, \tag{10}$$

where A_1 and A_3 are the complex amplitude functions for the fundamental mode with α and the third harmonic with 3α, respectively. We note here that all the coefficients involved in (9) as well as (10) are pure real. The set of equations (9) and (10) is a particular example $(m:n) = (1:3)$ of the general form obtained by Dangelmayr and Dangelmayr & Armbruster. Although the set of coupled amplitude equations is derivable from the method of multiple scales based on a small perturbation parameter which is a measure of the distance of (α, R) from the exactly resonating set $(1.7232445, 2573.739)$, we use the amplitude expansion method for the determination of the coefficients included in the set of equations (9) and (10) because we aim to obtain the equilibrium solutions of (9) and (10) even apart from the exact resonance parameter set. The correctness of the amplitude expansion method in the neighbourhood of the neutral state was discussed by Fujimura (1989) by making comparison with the method of multiple scales. We will also discuss the results of the amplitude expansion method by comparing them with that from the Fourier truncation method. We do not describe how all the coefficients are determined based on the amplitude expansion method because the expansion procedure is now routine (see Fujimura & Mizushima (1987), for example).

Now set

$$A_n(t) = a_n(t)\,\mathrm{e}^{\mathrm{i}\vartheta_n(t)} \quad (n = 1, 3), \quad \Theta = \vartheta_3 - 3\vartheta_1,$$

in order to reduce the degree of freedom from 4 to 3 as

$$\frac{\mathrm{d}a_1}{\mathrm{d}t} = c_1 a_1 + c_2 a_1^3 + c_3 a_1 a_3^2 + c_4 a_1^2 a_3 \cos\Theta, \tag{11}$$

$$\frac{\mathrm{d}a_3}{\mathrm{d}t} = d_1 a_3 + d_2 a_1^2 a_3 + d_3 a_3^3 + d_4 a_1^3 \cos\Theta, \tag{12}$$

$$\frac{\mathrm{d}\Theta}{\mathrm{d}t} = -(d_4 a_1^3 a_3^{-1} + 3c_4 a_1 a_3)\sin\Theta. \tag{13}$$

Equilibrium solutions of the set of equations (11)–(13) are given in Dangelmayr as equations (1.14) and (1.15) and can be classified into the following three categories:
(i) Pure mode solution (P):

$$a_1 = 0, \quad a_3^2 = -d_1/d_3.$$

This solution exists if $d_1 d_3 < 0$ and is stable if $c_1 < c_3 d_1/d_3$. The other pure mode solution ($a_1 \neq 0, a_3 = 0$) is impossible owing to the cubic terms in (9) and (10).
(ii) Mixed mode solution (M):

$$a_1 = r a_3, \quad a_3^2 = -d_1/(d_2 r^2 + d_3 + d_4 r^3 \cos\Theta),$$
$$\Theta = n\pi, \quad n = 0, \pm 1, \pm 2, \ldots,$$

where r is a root of

$$c_1 d_4 \cos\Theta r^3 + (c_1 d_2 - c_2 d_1) r^2 - d_1 c_4 \cos\Theta r + (c_1 d_3 - c_3 d_1) = 0.$$

The conditions of existence and stability of this solution are rather complicated, and will be discussed for a particular set of the values of parameters.
(iii) Travelling wave solution (T):

$$a_1^2 = -3c_4 d_4^{-1} a_3^2,$$

$$a_3^2 = \frac{3c_1 + d_1}{9c_2 c_4 d_4^{-1} - 3c_3 + 3c_4 d_2 d_4^{-1} - d_3},$$

$$\cos\Theta = -\frac{c_1 a_1 + c_2 a_1^3 + c_3 a_1 a_3^2}{c_4 a_1^2 a_3}.$$

The conditions of existence and stability of this solution are also complicated, and will be discussed for some examples of the values of parameters. It is seen at a glance that $c_4 d_4 < 0$ is necessary for this solution to exist.

We evaluated all the coefficients involved in (9) and (10) numerically and obtained the equilibrium solutions. The resultant bifurcation diagram is depicted for $P = 7.0$ and $R = 3000$, in terms of w_1, as the dashed line in figure 3. We find that the results from the cubic local equations agree well with those obtained from the Fourier truncation method not only qualitatively, but also quantitatively. The convergence of the amplitude expansion is very good, especially at small amplitude.

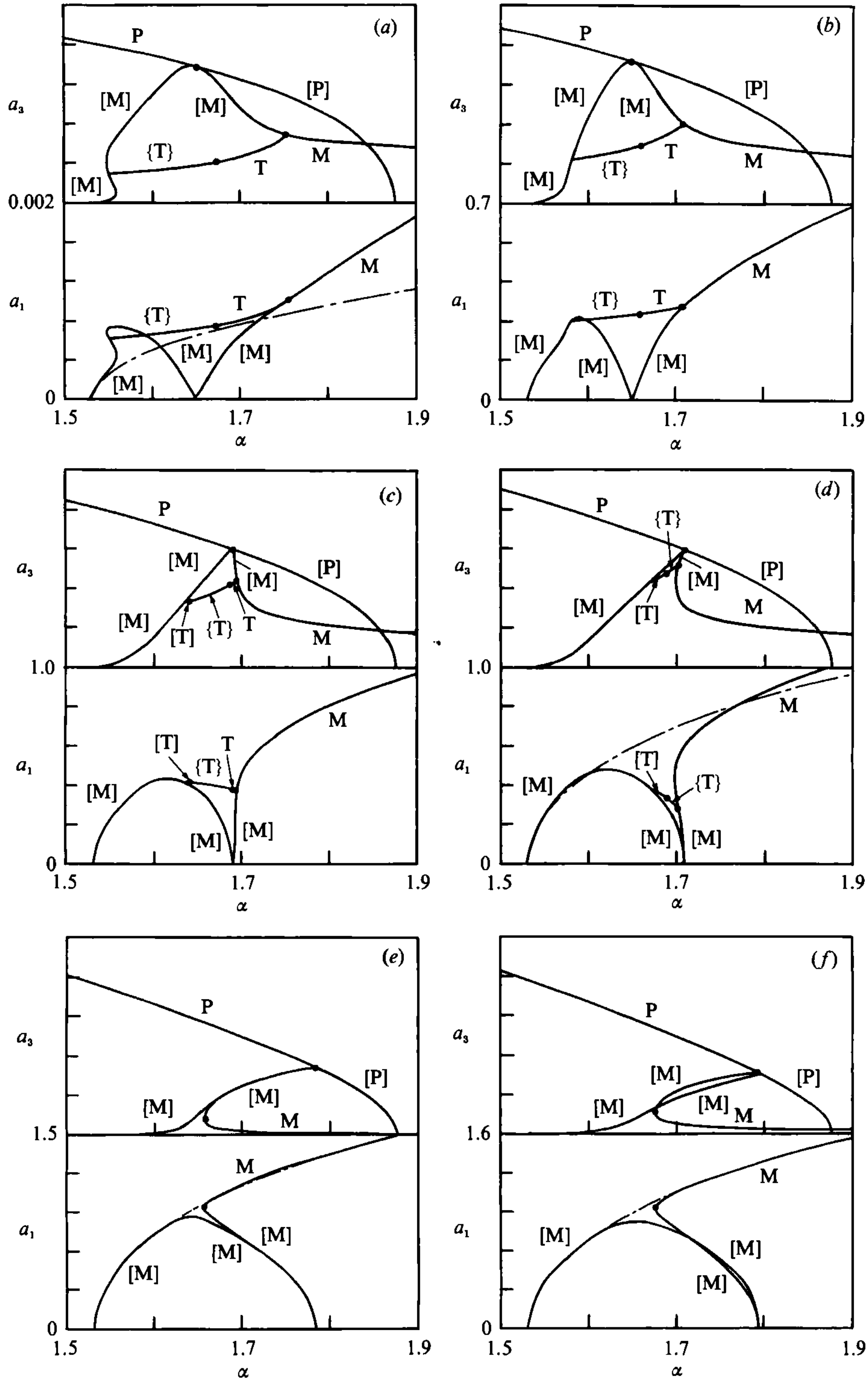

FIGURE 4. Branches of the equilibrium solution at $R = 3000$: P, pure mode; M, mixed mode; T, travelling wave. Modes without bracket are stable and the ones with [ ] are unstable. Modes with { } are unstable travelling modes bifurcating into stable modulated waves through Hopf bifurcation, depending on the parameter. The dash-dotted line denotes the equilibrium solution obtained from (8). (*a*) $P = 10^{-4}$, (*b*) $P = 0.05$, (*c*) $P = 0.1$, (*d*) $P = 0.12$, (*e*) $P = 0.7$, (*f*) $P = 10^3$.

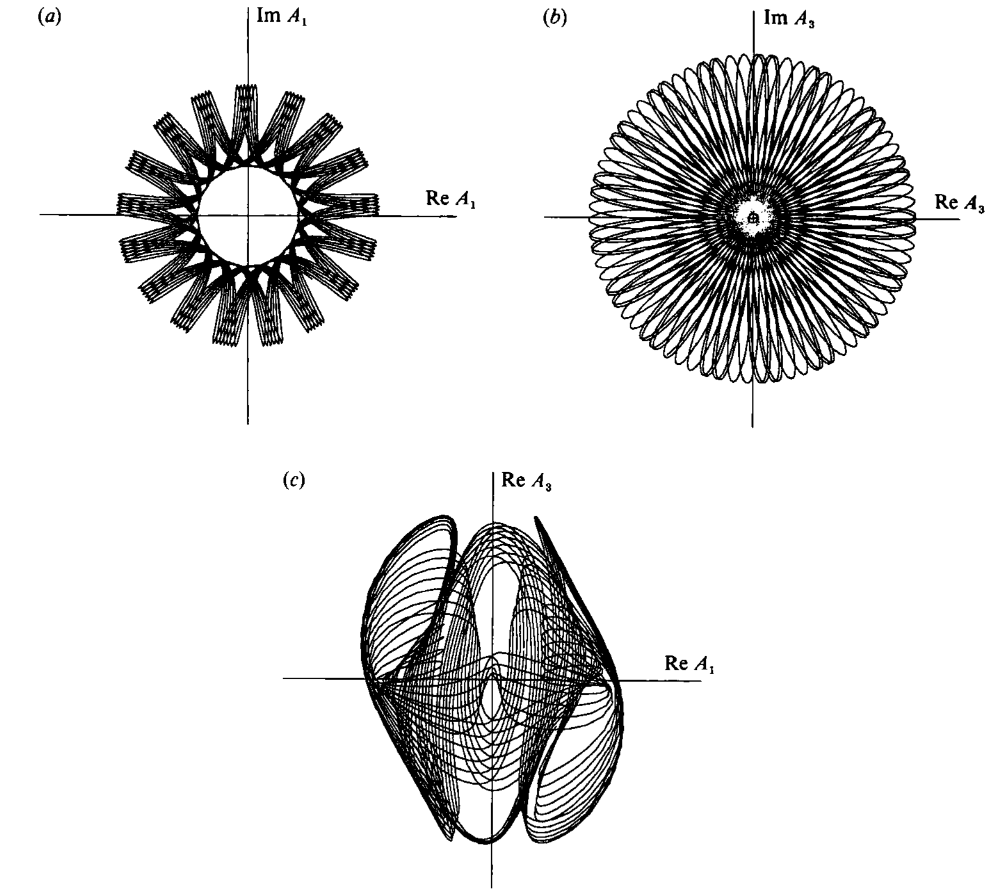

FIGURE 5(a–c). Phase diagrams of a stable modulated travelling wave solution for $(\alpha, P, R) = (1.66, 10^{-4}, 3000)$.

We show the bifurcation diagrams for $P = 10^{-4}$, 0.05, 0.1, 0.12, 0.7, and 10^3 at $R = 3000$ in figure 4(a–f). P, M, and T in these figures denote the pure mode, mixed mode, and travelling mode, respectively. Letters without bracket denote stable modes while letters bracketed by [ ] denote unstable modes and {T} denotes an unstable travelling wave which suffers from Hopf bifurcation and will be attracted by stable modulated waves depending on the value of the wavenumber. A typical modulated travelling wave is shown in figure 5 for $(\alpha, P, R) = (1.66, 10^{-4}, 3000)$. A travelling mode exists for $P \leqslant 0.12$ but not for $P \geqslant 0.13$. We list the coefficients of (9) and (10) in the limit of $P \rightarrow 0$ and $P \rightarrow \infty$ in table 3. Bifurcation diagrams have asymptotic forms for $P < 10^{-3}$ and $P > 10^2$. The asymptotic values of the equilibrium solutions for $P \ll 1$ are $10^4\,P$ times the equilibrium solutions for $P = 10^{-4}$ if $P < 10^{-3}$, while the values for $P \gg 1$ are the same as those for $P = 10^3$ if $P > 10^2$. Bifurcation characteristics for a finite Prandtl number will also be inferred from the table.

If the wavenumber α under consideration is much larger than the exactly resonating wavenumber $\alpha = \alpha_r$ $(= 1.7232445)$, the third harmonic is subcritical so that the harmonic can only affect the temporal evolution of the fundamental mode in $O(|A_1|^5)$. In such a case, the dynamics of the disturbance is governed by the Landau equation (8) for monochromatic mode. It is expected that the solution described by (8) changes into solutions described by (9) and (10) smoothly as $\alpha \downarrow \alpha_r$. Dash-dotted

$P \to \infty$ α	$\lambda_1 P$	λ_{-111}/P	λ_{-331}/P	λ_{-1-13}/P	$\lambda_3 P$	λ_{-113}/P	λ_{-133}/P	λ_{111}/P
1.50	−1.1370	−0.10076	−0.31427	−0.31719	18.490	0.0029923	−0.067175	0.17496
1.54	0.26624	−0.099427	−0.23996	−0.28701	16.764	−0.031026	−0.065938	0.17153
1.58	1.6502	−0.098134	−0.16247	−0.25580	14.965	−0.067910	−0.064494	0.16820
1.62	3.0127	−0.096886	−0.082319	−0.22355	13.100	−0.10772	−0.062814	0.16497
1.66	4.3515	−0.095683	−0.000053585	−0.19025	11.176	−0.15051	−0.060869	0.16184
1.70	5.6648	−0.094524	0.083716	−0.15589	9.2003	−0.19635	−0.058627	0.15880
1.74	6.9506	−0.093409	0.16832	−0.12043	7.1773	−0.24530	−0.056056	0.15586
1.78	8.2073	−0.092336	0.25301	−0.083870	5.1122	−0.29745	−0.053120	0.15301
1.82	9.4334	−0.091305	0.33700	−0.046193	3.0091	−0.35288	−0.049782	0.15025
1.86	10.628	−0.090316	0.41943	−0.0073805	0.87195	−0.41168	−0.045999	0.14759
1.90	11.788	−0.089368	0.49934	0.032581	−1.2967	−0.47397	−0.041727	0.14501

$P \to \infty$ α	λ_1	λ_{-111}	λ_{-331}	λ_{-1-13}	λ_3	λ_{-113}	λ_{-333}	λ_{111}
1.50	−0.35469	−1.2847	−5.6183	−0.59028	12.739	−8.4167	−7.2925	−0.28328
1.54	0.083980	−1.3271	−6.2018	−0.62413	11.775	−8.5175	−7.9017	−0.27622
1.58	0.52643	−1.3695	−6.8593	−0.66102	10.705	−8.6214	−8.5850	−0.26895
1.62	0.97212	−1.4118	−7.6026	−0.70135	9.5346	−8.7297	−9.3556	−0.26154
1.66	1.4205	−1.4541	−8.4458	−0.74561	8.2686	−8.8438	−10.230	−0.25402
1.70	1.8710	−1.4964	−9.4063	−0.79432	6.9128	−8.9651	−11.229	−0.24647
1.74	2.3231	−1.5387	−10.506	−0.84810	5.4721	−9.0952	−12.379	−0.23893
1.78	2.7761	−1.5811	−11.773	−0.90764	3.9518	−9.2354	−13.717	−0.23144
1.82	3.2297	−1.6237	−13.243	−0.97372	2.3566	−9.3871	−15.290	−0.22404
1.86	3.6830	−1.6663	−14.966	−1.0473	0.69131	−9.5518	−17.165	−0.21675
1.90	4.1357	−1.7091	−17.008	−1.1293	−1.0396	−9.7311	−19.436	−0.20960

TABLE 3. Coefficients involved in (9) and (10) for $R = 3000$

lines in figures 4(*a*), 4(*d*), 4(*e*), and 4(*f*) denote the equilibrium amplitudes evaluated from (8). It is obvious that the solution of (8) smoothly changes into solutions of (9) and (10) for $P > 0.7$ while these solutions are not connected smoothly for $P < 0.7$. We guess that much higher-order nonlinear interactions should be taken into account in the analysis for $P < 0.7$ in order to obtain a smooth connection between these curves.

4. Conclusion and discussion

A higher harmonic resonance between the quasi-neutral fundamental mode and the third harmonic with even symmetries is demonstrated to exist in Rayleigh–Bénard convection. Support of two-dimensional primary roll solutions is shown to shrink substantially as a result of the resonance mechanism. The coupled amplitude equations for the fundamental and the third harmonic which describe the resonant interaction between them are derived and all the coefficients involved in the equations are determined numerically. Bifurcation diagrams of the solutions are depicted for different values of the Prandtl number. It is shown that the pure mode and mixed modes exist for relatively high-Prandtl-number fluids while the pure mode, mixed modes, travelling waves, and modulated waves exist for relatively low-Prandtl-number fluids. The mixed mode and travelling wave solutions have been obtained by Dangelmayr (1986) as solutions of the normal form in the presence of $O(2)$-symmetry.

Let us now discuss physical significance of the new type of solution obtained in the present paper. The primary roll solutions with which Busse & Clever examined the secondary instabilities are correct. However, they examined only the stable equilibrium solutions (upper branch of the diagram for the equilibrium solutions) which consist of the pure mode and mixed mode solutions, although they did not distinguish between them. We have shown that there is another branch of the primary roll solutions, i.e. the unstable pure mode and unstable mixed mode solutions. The solutions can be observed experimentally for a certain period of time if a disturbance happens to have a similar form to the unstable pure mode or mixed mode solutions. Since the secondary stability of the unstable primary solutions has not been examined yet, we cannot predict a final pattern of the unstable primary rolls for $t \rightarrow \infty$. It might thus be insufficient to predict the bifurcation of the primary solutions only using Busse's balloon although the balloon is correct as the stability boundary for stable and steady equilibrium rolls. The existence of the parameter region where the fundamental mode decays while the third harmonic survives as a stable pure mode leads changes the implications of Busse's balloon. Take $P = 7.0$ and $R = 6000 \leqslant R \leqslant 15000$ for example. It is expected from Busse's balloon that the roll with $\alpha = 1$ will develop to an equilibrium one and that the roll is unstable to cross-roll instability. According to present results, the roll with $\alpha = 1$ will decay before it attains to its equilibrium state but excite the third harmonic which develops to an equilibrium roll with $\alpha = 3$. The roll with $\alpha = 3$ is stable to any two- or three-dimensional disturbances, judging from Busse's balloon. Our results therefore predict that the roll with $\alpha = 1$ develops eventually to the stable equilibrium one with $\alpha = 3$. The stability of the travelling wave solutions has not been examined yet. It is not therefore confirmed whether if the solution is physically achievable.

We obtained the bifurcation diagrams for the primary roll solutions in a horizontal layer with infinite extent. If the fluid is confined between horizontal plates with annular geometry and appropriate lateral circular boundaries, all the solutions obtained there will be free from the Eckhaus instability. The latter physical set-up is therefore advantageous when we interpret the physical significance of the diagrams obtained.

Now, we briefly describe a different class of strong nonlinear interaction between three even-symmetric modes, i.e. the fundamental, the second harmonic, and the third harmonic. Suppose that the fundamental and the third harmonic are in a resonant relation. The second harmonic with even symmetry is then in a supercritical state with a large linear growth rate. Actually, the mode is almost the fastest growing mode for the Rayleigh number considered there. The mode thus dominates the dynamics in a short timescale. We thus need to take account of the contribution of the second harmonic with even symmetry. We describe briefly a preliminary analysis in the Appendix. Complete analysis is possible only through the numerical calculation of the global bifurcation characteristics based on the Fourier truncation method and will be a subject of our future work.

Finally, we mention an important different physical set-up: convection in a horizontal fluid layer between a rigid boundary and a stress-free boundary. As Armbruster (1987) has already pointed out, the spatial symmetry in the z-direction is broken from the beginning just as the case considered by Busse (1987). The dynamics is thus governed by coupled amplitude equations of the form

$$\frac{\mathrm{d}A_1}{\mathrm{d}t} = \lambda_1 A_1 + \lambda_{-12} A_1^* A_2 + \lambda_{-111} |A_1|^2 A_1 + \lambda_{-221} |A_2|^2 A_1,$$

$$\frac{\mathrm{d}A_2}{\mathrm{d}t} = \lambda_2 A_2 + \lambda_{11} A_1^2 + \lambda_{-112} |A_1|^2 A_2 + \lambda_{-222} |A_2|^2 A_2,$$

where A_1 and A_2 are complex amplitude functions of the fundamental and the second harmonic, respectively. The equations have been investigated extensively for their bifurcation characteristics and dynamical responses by Dangelmayr (1986), Dangelmayr & Armbruster (1986), Knobloch & Proctor (1988), and Proctor & Hughes (1990) and we do not discuss them further in the present paper.

Appendix. 1:2:3 strong nonlinear interaction

In the main body of the present paper, we excluded an even-symmetric second harmonic and pointed out that the 1:3 resonance takes place in Rayleigh–Bénard convection. We consider in this Appendix the effect of the second harmonic as mentioned at the end of §4.

Let us select a parameter set in the neighbourhood of the exactly resonating one $(\alpha, R) = (1.7232445, 2573.739)$ and imagine that the fundamental mode and the third harmonic are in quasi-neutral states, again. We then introduce the even-symmetric second harmonic. The harmonic can be regarded as the most unstable mode because the wavenumber of the second harmonic, 3.446, is quite close to the wavenumber $\alpha_{\max}$ of the most unstable mode: $\alpha_{\max} = 3.188$ for $(P, R) = (10^{-4}, 3000)$, 3.302 for (0.1, 3000), 3.518 for (1, 3000), or 3.632 for (1000, 3000). The co-existence of these three even-symmetric modes is thus easily interpreted as the existence of the most unstable mode associated with its subharmonics. Global bifurcation characteristics for such a situation can only be obtained through the Fourier truncation method because the second harmonic is far from the linearly critical state. Here, however, we presume that the Rayleigh number under consideration, $R \geqslant 2574$, is *sufficiently close to the critical value* 1707.762, or more specifically, $R - R_c \ll R_c$, that a nonlinear interaction among these three modes can be regarded as a new class of nonlinear *resonance* with wavenumber ratio 1:2:3. The amplitude equations for the latter case are then easily inferred as

$$\left.\begin{aligned} \frac{dA_1}{dt} &= b_1 A_1 + b_2 |A_1|^2 A_1 + b_3 |A_2|^2 A_1 + b_4 |A_3|^2 A_1 + b_5 A_1^{*2} A_3 + b_6 A_2^2 A_3^*, \\ \frac{dA_2}{dt} &= c_1 A_2 + c_2 |A_1|^2 A_2 + c_3 |A_2|^2 A_2 + c_4 |A_3|^2 A_2 + c_5 A_1 A_2^* A_3, \\ \frac{dA_3}{dt} &= d_1 A_3 + d_2 |A_1|^2 A_3 + d_3 |A_2|^2 A_3 + d_4 |A_3|^2 A_3 + d_5 A_1^3 + d_6 A_1^* A_2^2. \end{aligned}\right\} \quad \text{(A 1)}$$

Derivation of (A 1) in a rigorous fashion is impossible without utilizing the centre-unstable manifold reduction adopted in the analysis of the Kuramoto–Sivashinsky equation by Armbruster, Guckenheimer & Holmes (1989) which still needs further work for its mathematical justification if the parameter set is far from the bifurcation point. Instead, we assumed the form of (A 1) *a priori* and determined the numerical values of all the coefficients involved there based on the usual amplitude expansion technique.

Set $A_n(t) = a_n(t)\, e^{i\vartheta_n(t)}$ ($n = 1, 2,$ and 3), $\Theta_1 \equiv \vartheta_3 - 3\vartheta_1$, and $\Theta_2 \equiv 2\vartheta_2 - \vartheta_1 - \vartheta_3$. Then, added to the possible solutions for 1:3 resonance obtained in §3 (again, we refer the pure mode, the mixed mode, and the travelling wave obtained for the 1:3 resonance as P, M, and T, respectively), we obtain the following three new solutions: (*a*) a pure mode solution (P2):

$$a_1 = a_3 = 0, \quad a_2^2 = -c_1/c_3;$$

(*b*) a mixed mode solution (M2):

$$a_1^2 = -\frac{p_2 + p_4 r + p_3 r^2 + p_6 r^3}{p_1 + p_5 r}, \quad a_3 = a_1 r,$$

$$a_2^2 = -c_3^{-1}(c_1 + c_2 a_1^2 + c_4 a_3^2 + \tilde{c}_5 a_1 a_3),$$

$$\Theta_1 = \Theta_2 = 0; \quad \Theta_1 = \Theta_2 = \pi; \quad \Theta_1 = 0, \Theta_2 = \pi; \quad \text{or} \quad \Theta_1 = \pi, \Theta_2 = 0,$$

where

$$\begin{gathered} p_1 = b_1 - c_3^{-1} b_3 c_1, \quad p_2 = b_2 - c_3^{-1} b_3 c_2, \quad p_3 = b_4 - c_3^{-1}(b_3 c_4 + \tilde{b}_6 \tilde{c}_5), \\ p_4 = \tilde{b}_5 - c_3^{-1}(b_3 \tilde{c}_5 + \tilde{b}_6 c_2), \quad p_5 = -c_3^{-1} \tilde{b}_6 c_1, \quad p_6 = -c_3^{-1} \tilde{b}_6 c_4, \\ q_1 = d_1 - c_3^{-1} d_3 c_1, \quad q_2 = d_2 - c_3^{-1}(d_3 c_2 + d_6 \tilde{c}_5), \quad q_3 = d_4 - c_3^{-1} d_3 c_4, \\ q_4 = \tilde{d}_5 - c_3^{-1} \tilde{d}_6 c_2, \quad q_5 = -c_3^{-1} \tilde{d}_6 c_1, \quad q_6 = -c_3^{-1}(d_3 \tilde{c}_5 + \tilde{d}_6 c_4), \\ \tilde{b}_5 \equiv b_5 \cos\Theta_1, \quad \tilde{b}_6 \equiv b_6 \cos\Theta_2, \quad \tilde{c}_5 \equiv c_5 \cos\Theta_2, \quad \tilde{d}_5 \equiv d_5 \cos\Theta_1, \quad \tilde{d}_6 \equiv d_6 \cos\Theta_2, \end{gathered}$$

and r satisfies

$$\begin{aligned} (p_6 q_1 - p_5 q_3) r^4 + (p_6 q_5 + p_3 q_1 - p_1 q_3 - p_5 q_6) r^3 + (p_3 q_5 + p_4 q_1 - p_1 q_6 - p_5 q_2) r^2 \\ + (p_2 q_1 + p_4 q_5 - p_1 q_2 - p_5 q_4) r + (p_2 q_5 - p_1 q_4) = 0; \end{aligned}$$

(*c*) a travelling wave solution (T2):

$$a_1 a_2 a_3 \neq 0, \quad \Theta_1 \neq 0, \pi; \quad \Theta_2 \neq 0, \pi.$$

It is impossible to give the explicit form of the travelling wave solution T2, so we adopted the Newton–Raphson method to calculate it by using random numbers for an initial guess of the numerical iteration.

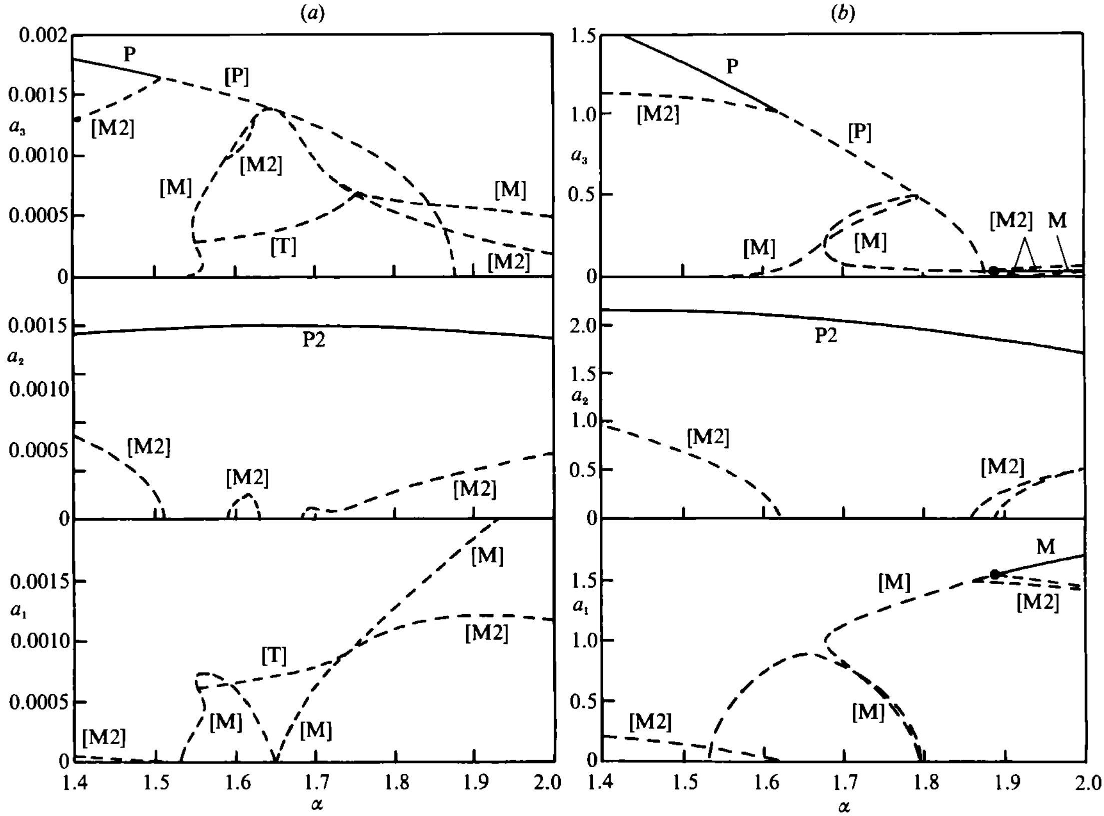

FIGURE 6. Bifurcation diagrams for the 1:2:3 interaction at $R = 3000$. P2, pure mode; M2, mixed mode. For P, M, T, and the meaning of the bracket, see caption to figure 4. (*a*) $P = 10^{-4}$, (*b*) $P = 1000$.

We depicted typical bifurcation diagrams in figures 6(*a*) and 6(*b*) for $1.4 \leqslant \alpha \leqslant 2.0$ with $R = 3000$ at $P = 10^{-4}$ and 1000, respectively. We can conclude from these figures that all the mixed mode solutions M2 are unstable. The travelling wave solutions categorized as T2 are obtained only in a high-wavenumber range for $P < 0.08$: $\alpha \geqslant 2.064$ for $P = 10^{-4}$ and $P = 10^{-3}$, $\alpha \geqslant 2.074$ for $P = 10^{-2}$, $\alpha \geqslant 2.090$ for $P = 0.02$, $\alpha \geqslant 2.146$ for $P = 0.04$, $\alpha \geqslant 2.257$ for $P = 0.06$, and $\alpha \geqslant 2.386$ for $P = 0.07$. They are however found to be unstable. All the travelling wave solutions for the 1:3 resonance (T) are also unstable according to (A 1).

It is found that the pure mode solution P2 is always stable while the pure mode solution for 1:3 resonance (P) is partly stable. The mixed mode solutions for 1:3 resonance, M, attain stability for a relatively high wavenumber and Prandtl number range as is shown in figure 7. If we superimpose the subharmonic with $\alpha = \frac{1}{2}\alpha_{\max}$ onto the most unstable mode, then the nonlinear interaction between $\alpha_{\max}$ and $\frac{1}{2}\alpha_{\max}$ modes generates the $\frac{3}{2}$th-harmonic with $\alpha = \frac{3}{2}\alpha_{\max}$ at the cubic order. If the amplitudes of the subharmonics are large enough, the nonlinear interaction between these two subharmonics will dominate the dynamics and the mixed mode solution (M) will be attained. Otherwise, the P2 solution will dominate the dynamics.

The pure mode solutions P and P2 have been examined by Busse and his co-workers for their secondary instability. The physical realizability of the pure more solutions is thus governed by Busse's balloon. The P2 solution seems to be inside the balloon while the stable P solution will be outside for the R considered here. The stable mixed

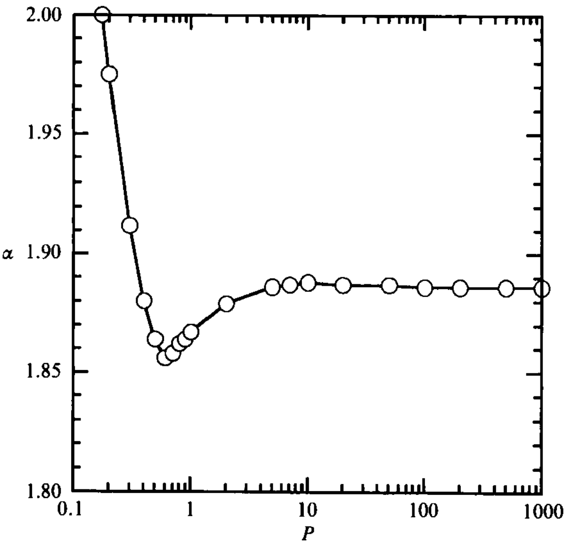

FIGURE 7. Stability boundary of the mixed mode M in the case of the 1:2:3 interaction. The mixed mode is stable above the boundary.

mode solution for the 1:3 resonance (M), on the other hand, has not been examined yet for its secondary instability. If the mixed mode solution is stable to all the two- and three-dimensional disturbances, then the most unstable mode and the mixed mode can coexist. But before further discussing the physical significance of the stable mixed mode solution, we need to analyse the global bifurcation as well as the secondary instability of 1:2:3 interaction systems by taking account of the even-symmetric mode with $\alpha \approx \alpha_{max}$.

REFERENCES

ARMBRUSTER, D. 1987 $O(2)$-symmetric bifurcation theory for convection rolls. *Physica* **27D**, 433–439.

ARMBRUSTER, D., GUCKENHEIMER, J. & HOLMES, P. 1989 Kuramoto–Sivashinsky dynamics on the centre-unstable manifold. *SIAM J. Appl. Maths* **49**, 676–691.

BUSSE, F. H. 1967 On the stability of two-dimensional convection in a layer heated from below. *J. Maths and Phys.* **46**, 140–150.

BUSSE, F. H. 1987 Transition to asymmetric convection rolls. In *Bifurcation: Analysis, Algorithms, Applications* (ed. T. Küpper, R. Seydel & H. Troger), pp. 18–26. Birkhäuser.

BUSSE, F. H. & CLEVER, R. M. 1979 Instabilities of convection rolls in a fluid of moderate Prandtl number. *J. Fluid Mech.* **91**, 319–335.

BUSSE, F. H. & OR, A. C. 1986 Subharmonic and asymmetric convection rolls. *Z. Angew. Math. Phys.* **37**, 608–623.

BUSSE, F. H. & WHITEHEAD, J. A. 1971 Instabilities of convection rolls in a high Prandtl number fluid. *J. Fluid Mech.* **47**, 305–320.

CLEVER, R. M. & BUSSE, F. H. 1974 Transition to time-dependent convection. *J. Fluid Mech.* **65**, 625–645.

DANGELMAYR, G. 1986 Steady-state mode interactions in the presence of $O(2)$-symmetry. *Dyn. Stab. Syst.* **1**, 159–185.

DANGELMAYR, G. & ARMBRUSTER, D. 1986 Steady-state mode interactions in the presence of $O(2)$-symmetry and in non-flux boundary value problems. *Contemp. Maths* **56**, 53–67.

FUJIMURA, K. 1989 The equivalence between two perturbation methods in weakly non-linear stability theory for parallel shear flows. *Proc. R. Soc. Lond.* A **424**, 373–392.

Fujimura, K. & Mizushima, J. 1987 Nonlinear interaction of disturbances in free convection between vertical parallel plates. In *Nonlinear Wave Interactions in Fluids* (ed. R. W. Miksad, T. R. Akylas & T. Herbert), pp. 123–130. ASME.

Jeffreys, H. 1928 Some cases of instability in fluid motion. *Proc. R. Soc. Lond.* A **118**, 195–208.

Kidachi, H. 1982 Side wall effect on the pattern formation of the Rayleigh–Bénard conveetion. *Prog. Theor. Phys.* **68**, 49–63.

Knobloch, E. & Guckenheimer, J. 1983 Convective transitions induced by a varying aspect ratio. *Phys. Rev.* A **27**, 408–417.

Knobloch, E. & Proctor, M. R. E. 1988 The double Hopf bifurcation with 2:1 resonance. *Proc. R. Soc. Lond.* A **415**, 61–90.

Li, R. 1986 Analysis for Taylor vortex flow. Ph.D. thesis, Virginia Polytechnic Institute.

Meyer-Spasche, R. & Keller, H. B. 1985 Some bifurcation diagrams for Taylor vortex flows. *Phys. Fluids* **28**, 1248–1252.

Mizushima, J. & Saito, Y. 1988 Equilibrium characteristics of the secondary convection in a vertical fluid layer between two flat plates. *Fluid Dyn. Res.* **2**, 183–191.

Nagata, M. & Busse, F. H. 1983 Three-dimensional tertiary motions in a plane shear layer. *J. Fluid Mech.* **135**, 1–26.

Pellew, A. & Southwell, R. V. 1940 On maintained convective motion in a fluid heated from below. *Proc. R. Soc. Lond.* A **176**, 312–343.

Proctor, M. R. E. & Hughes, D. W. 1990 Chaos and the effect of noise for the double Hopf bifurcation with 2:1 resonance. In *Nonlinear Evolution of Spatio-Temporal Structures in Dissipative Continuous Systems* (ed. F. H. Busse & L. Kramer), pp. 375–384. Plenum.

Reid, W. H. & Harris, D. L. 1958 Some further results on the Bénard problem. *Phys. Fluids* **1**, 102–110.

Schlüter, A., Lortz, D. & Busse, F. H. 1965 On the stability of steady finite amplitude convection. *J. Fluid Mech.* **23**, 129–144.

Specht, H., Wagner, M. & Meyer-Spasche, R. 1989 Interactions of secondary branches of Taylor vortex solutions. *Z. Angew. Math. Mech.* **69**, 339–352.